ADVANCED FUNCTIONAL MATERIALS
www.afm-journal.de

Cooperative Liquid Crystal Photo-Polymerization and -Alignment with In Situ Monitoring for Substrate Independent Patterning of Optical Anisotropy

*Joy Zhou, Jinwon Seo, Yudian Wu, Cedric P. Ambulo, Zachary M. Marsh, Kyungmin N. Lee, Nicholas P. Godman, and Zachariah A. Page**

Spatial control over molecular order in polymeric systems will enable advancements in healthcare and photonics, from soft actuators to data storage and encryption. Liquid crystalline (LC) materials are attractive for their intrinsic combination of long-range anisotropy and fluidity that enables alignment. Photoalignment represents an attractive noncontact ordering mechanism. However, contemporary hurdles preventing widespread implementation of photoalignment include the use of high-intensity light sources, restrictions to thin films (<1 µm) and specific substrates, multistep LC syntheses, and costly processing. Herein, an interplay between photo-polymerization and -alignment with commercially relevant LCs is reported. Systematic, in situ monitoring of optical anisotropy using a custom microscopy setup provides unique mechanistic insight and facilitates optimization. The optimized process occurs rapidly (<10 min) from an isotropic state with a one-step exposure to low-intensity blue linearly polarized light. As a result, substrate-independent photoalignment of thick (≈6–38 µm), optically transparent LC networks is demonstrated, along with a wide LC-matrix scope that includes thiol-containing elastomers. Furthermore, photopatterning provides excellent fidelity (<5 µm) and access to complex images with multiangle optical anisotropy. This user-friendly process will facilitate production of "smart" (stimuli-responsive) plastics for improved human health and information security.

1. Introduction

Light as an energy source provides spatiotemporal control over creating and/or manipulating soft, stimuli-responsive (i.e., "smart") materials, with applications ranging from wearable electronics and soft robotics to data storage and encryption.[1–5] Among these "smart" materials, liquid crystals (LCs) are unique in their molecular level control over order (direction/position), which has brought about modern optoelectronic technologies including the ubiquitous liquid crystal display (LCD).[6–10] Despite the industrialization of LCs over 30 years ago, nascent challenges and opportunities exist with respect to unrestricted control over molecular ordering. These challenges primarily arise from limitations with contemporary alignment methods, which can generally be categorized as contact (e.g., mechanical rubbing) and noncontact (e.g., light-induced).[11–16] The advent of a universal and mild LC alignment method is thus anticipated to result in advanced "smart" plastics with tailored properties (optical, mechanical, thermal, etc.) that enable new and/or improved healthcare, optics, and photonics technologies.[17–24]

Light-induced alignment (photoalignment) offers distinct advantages over mechanical rubbing, the standard method to produce LCDs today.[11,15,16] Notably, photoalignment is a noncontact method that precludes particle/fiber contamination, defects (e.g., scratches), and electrostatic charges on the surface that occur from mechanical rubbing. Additionally, photoalignment enables patterned anisotropy through spatially localized irradiation[25] (**Figure 1**A). Since its first discovery in 1988 by Seki et al.,[26] photoalignment via light-driven *E*/*Z*-isomerization of azobenzene and its derivatives represents the most widely studied strategy. This is due in-part to the accessibility and synthetic modularity of azobenzene's chemical structure and concomitant photophysical properties (e.g., light absorption, solubility, and *E*/*Z* switching kinetics).[27] The principally accepted photoalignment mechanism for azo-compounds is known as the Weigert effect.[28] In this mechanism, absorption of linearly

J. Zhou, J. Seo, Y. Wu, Z. A. Page
Department of Chemistry
The University of Texas at Austin
Austin, TX 78712, USA
E-mail: zpage@cm.utexas.edu
C. P. Ambulo, Z. M. Marsh, K. N. Lee, N. P. Godman
Materials and Manufacturing Directorate
Air Force Research Laboratory
Wright-Patterson AFB
Ohio 45433, USA
C. P. Ambulo, Z. M. Marsh, K. N. Lee
Azimuth Corporation
Fairborn, Ohio 45324, USA

The ORCID identification number(s) for the author(s) of this article can be found under https://doi.org/10.1002/adfm.202308828

DOI: 10.1002/adfm.202308828

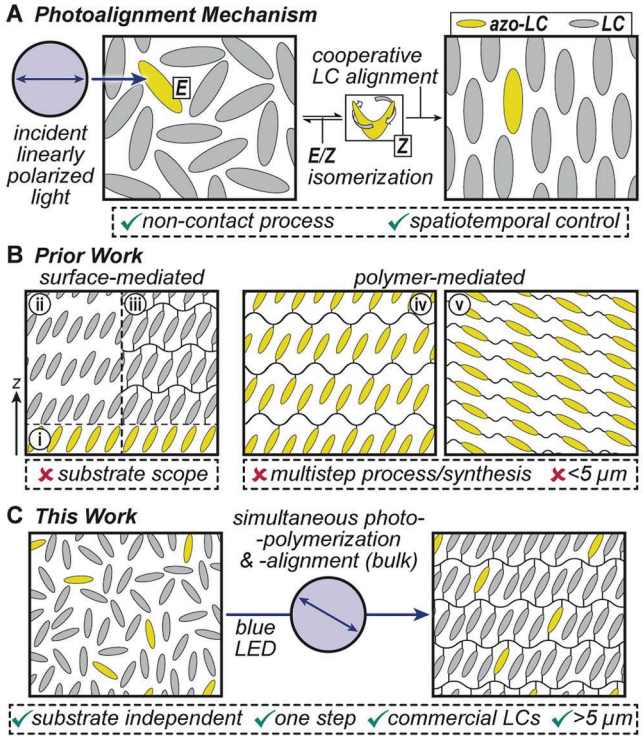

Figure 1. A) General mechanism for alignment via photoisomerization with linearly polarized light. B) State-of-the-art surface- and polymer-mediated photoalignment approaches. Surface-mediated relies on (i) photoalignment of an azo-coated surface (command layer), (ii) casting of LCs onto the surface, and (iii) polymerization to fix LC order. Polymer-mediated photoalignment is accomplished by synthesizing polymers containing azo-functionality in the (iv) side-chain or (v) main-chain. "x" represents limitations. C) Present work showcasing a user-friendly and versatile one-step photoalignment strategy from commercial LCs. LC = liquid crystal; LED = light emitting diode.

polarized light (LPL) results in successive *E*/*Z*-isomerization and molecular reorientation until the transition dipole moment of the azo-compound – typically parallel to the long molecular axis – is perpendicular to the electric field vector of light (Figure 1A). In this orientation, no further absorption of the LPL occurs, essentially fixing the azobenzene that is capable of cooperatively reorienting surrounding LCs to produce long-range order.

In practice, LC photoalignment has been applied to surface- and polymer-mediated methods, wherein azobenzene is anchored to a substrate or macromolecular chain, respectively (Figure 1B). Alternatively, scanning-wave photoalignment has been demonstrated as a dye-free route to LC patterning, yet it requires a specialized setup for light-rastering.[29,30] In both surface- and polymer-mediated processes, photoalignment is often accomplished using LPL exposure of samples in the nematic mesophase (i.e., elevated temperatures),[31] where the presence of directional order, yet lack of positional order enables cooperative molecular reorientation. Additionally, photo-alignment and/or -polymerization are often (although not exclusively[32]) accomplished using multistep high energy (UV) and/or intensity (≥100 mW cm^{-2}) irradiation,[11,15] providing opportunities for improvement.

In surface-mediated photoalignment, photoresponsive units (e.g., azo-compounds) are anchored to the surface, either through direct covalent attachment or adsorption, and irradiated with LPL[33–36] (Figure 1Bi). Subsequently, a nonphotoresponsive LC matrix, such as 4′-pentyl-4-biphenylcarbonitrile (5CB) or 4′-pentyl-4-biphenylcarbonitrile (E7), is placed onto the photoaligned layer (e.g., commanding surface), and orients to it (Figure 1Bii). If using reactive mesogens (e.g., acrylate-functionalized LCs), the alignment can be fixed via a secondary polymerization (crosslinking) step, often using UV light (Figure 1Biii).[37–41] The surface-based method offers good control over LC alignment, yet challenges include time-consuming multistep processing as described above, and constraints in LC matrix thickness (<50 μm).[42–44] Additionally, requisite surface treatment precludes direct contact of the bulk LC matrix to various functional substrates (e.g., conductive ITO-coated glass), limiting end-use applications.

In analogy to the surface method, polymer-mediated photoalignment has been achieved most commonly through covalent attachment of the photoresponsive unit to a polymer as a side-chain[45–50] (Figure 1Biv) or main-chain unit[32,51–53] (Figure 1Bv). This facilitates alignment by cooperative motion between the azo motif and polymer chain, which results in a higher energy barrier to molecular reorientation in both the forward (order) and reverse (disorder) directions. In turn polymer-mediated photoalignment often requires higher energy dosages (≈10 J cm^{-2})[53,54] relative to analogous small molecule surface-mediated processes. The benefits of polymer-mediated photoalignment are the expanded substrate scope and process simplicity (single step and ease of surface coating). However, the synthetic complexity of photoresponsive polymers (and their precursors) to date has precluded the scale-up necessary for widespread implementation. Moreover, light attenuation from high-density azobenzene functionalization common to these systems restricts sample thickness (<1 μm). Such thin films preclude application in emergent additive manufacturing technologies that use >5 μm layers (e.g., stereolithography), while minimizing the potential work output useful in soft actuator applications.[42,54]

Taken together, an ideal photoalignment process 1) uses a mild and efficient visible light source (e.g., LED, < 100 mW cm^{-2}), 2) occurs rapidly (e.g., <10 min), 3) requires only a single step, 4) is independent of substrate composition, and 5) works with a range of thicknesses and accessible/scalable LCs. This objective is accomplished herein with a user-friendly photopolymerization and -alignment strategy described generally as a "bulk" process, given that it operates with a thick (>5 μm) mixture (i.e., resin) comprising a photoresponsive azo compound diluted in an LC host matrix (Figure 1C). Uniquely, the entire process unfolds from an isotropic state via a one-step irradiation (≈3–10 min) using relatively low intensity (≈30–90 mW cm^{-2}) blue LPL exposure generated by inexpensive thin-film polarizes and a commercial LED. A systematic examination of factors that influence the degree of optical anisotropy is made possible via in situ monitoring with a distinctive, yet accessible polarized optical microscope (POM) setup. The substrate independence, wide LC matrix scope, feature resolution, and multi-angle photopatterning of the present process are showcased. This report provides a blueprint to facilitate patterning of complex optical anisotropy and mechanistic insight that will

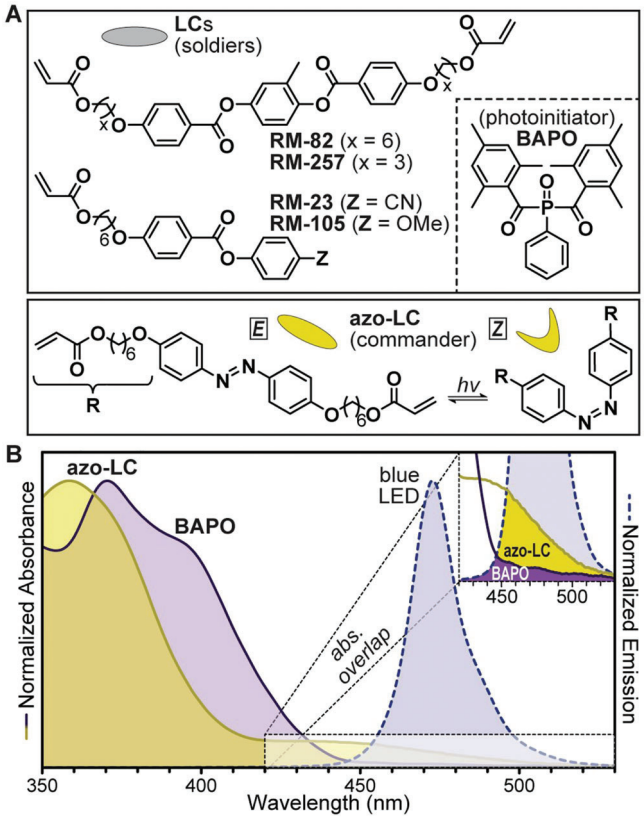

Figure 2. A) Chemical structures for LCs and photoinitiator. B) Overlay of normalized UV-vis absorption and LED emission spectra, showing the overlap between azo-LC and BAPO. RM = reactive mesogen; BAPO = bisacylphosphine oxide.

enable further optimization and derivatization of this modular photoalignment process towards next-generation "smart" plastics.

2. Results and Discussion

2.1. LC Matrix Design

The LC matrix comprised two commercially available acrylate-terminated phenylester derivatives, known colloquially as reactive mesogens (RMs), specifically RM-82 or RM-257 and RM-23 or RM-105 (**Figure 2**A). The combination of RM-82 or RM-257 (diacrylate) and RM-23 or RM-105 (monoacrylate) was initially selected given the low cost and precedent to provide an LC matrix with a wide nematic window[55] (≈75—97 °C, Figure S4, Supporting Information). Bisacylphosphine oxide (BAPO) was selected as a classic Type I photoinitiator to induce polymerization (i.e., curing) upon activation with ≈365–405 nm (UV-violet) irradiation. To examine the effect of azobenzene functionality on photoalignment, we initially examined 8 different acrylate-functionalized derivatives (Scheme S1 and Figures S5–S6, Supporting Information). The first photoalignment experiments were accomplished by mixing the components in a 61:30:9 ratio for RM-82:RM-23:azobenzene, respectively, with 2–4 wt% BAPO (Figures S5, Supporting Information). This mixture provided a nematic-to-isotropic mesophase transition temperature (T_{NI}) of 97 °C as measured using a POM (Figure S4A, Supporting Information). The mixture was then heated to an isotropic temperature (105 °C) using a transparent ITO-coated quartz heater, followed by injection between two nontreated glass microscope slides that were separated by 38 µm plastic shims (Figures S5–S7, Supporting Information). Samples were subsequently photoaligned (30 mW cm^{-2} at sample surface) for 10 min with a blue LED centered at 470 nm (Figure 2B) that had been passed through a linear polarizer. After the initial irradiation, samples were cooled to 75 °C (nematic mesophase), and irradiated with a UV LED centered at 365 nm to induce curing (Figure S5, Supporting Information). Of the 8 azobenzene derivatives, the diacrylate azobenzene with hexamethylene spacers (Figure 2A) provided the largest change in brightness between crossed-polarizers (Figure S6, Supporting Information). This optical anisotropy was indicative of successful photoalignment. For clarity, the remainder of the results will focus solely on this particular azobenzene derivative, referred to herein as "azo-LC".

At this stage, we hypothesized that photoalignment occurred upon entering the nematic mesophase upon cooling, with molecular order being locked-in via curing with subsequent UV exposure. However, performing control experiments where the samples were held at 105 °C (i.e., not cooled) provided qualitatively similar optical anisotropy. In contrast, turning the blue LED on only after cooling the sample from isotropic to the nematic mesophase (≈80—95 °C) resulted in no observable optical anisotropy (Figures S8–S9, Supporting Information). Furthermore, blue LPL and the nonphotoresponsive LC matrix were both necessary to achieve measurable optical anisotropy (Figures S8–S9 and Videos S1, S2, Supporting Information). Additionally, photocuring appeared to proceed in the absence of UV light irradiation, as evidenced by the formation of a solid film with only blue light exposure. Carefully measuring UV-vis absorption for both azo-LC and BAPO revealed a small absorption cross-section of each component with the blue LED emission profile (Figure 2B). Quantifying molar absorptivity revealed values of 12 340 and 760 M^{-1} cm^{-1} at 470 nm, respectively (Figure S12, Supporting Information). Considering their relative concentrations, it was calculated that azo-LC (9 wt%) absorbs ≈200–100× more photons than BAPO (≈2–4 wt%) across the blue LED spectral profile (Figures S13–S14, Supporting Information). Taken together, the new hypothesis was that photo-polymerization and -alignment were occurring simultaneously, despite starting in an isotropic state.

2.2. Monitoring Photo-Alignment

To test this new conjecture, we developed a custom POM setup that enabled in situ activation and monitoring of photoalignment (**Figure 3**A). In short, samples were placed on a temperature-controlled stage and simultaneously irradiated with red LPL (bottom-up) to avoid absorption by the photoinitiator and azo-LC. The blue LPL was set to 45° relative to the red light, and it was passed through a size-adjustable iris with a hexagonal opening prior to hitting the sample (top-down). The isotropic (dark) background surrounding the hexagonally irradiated

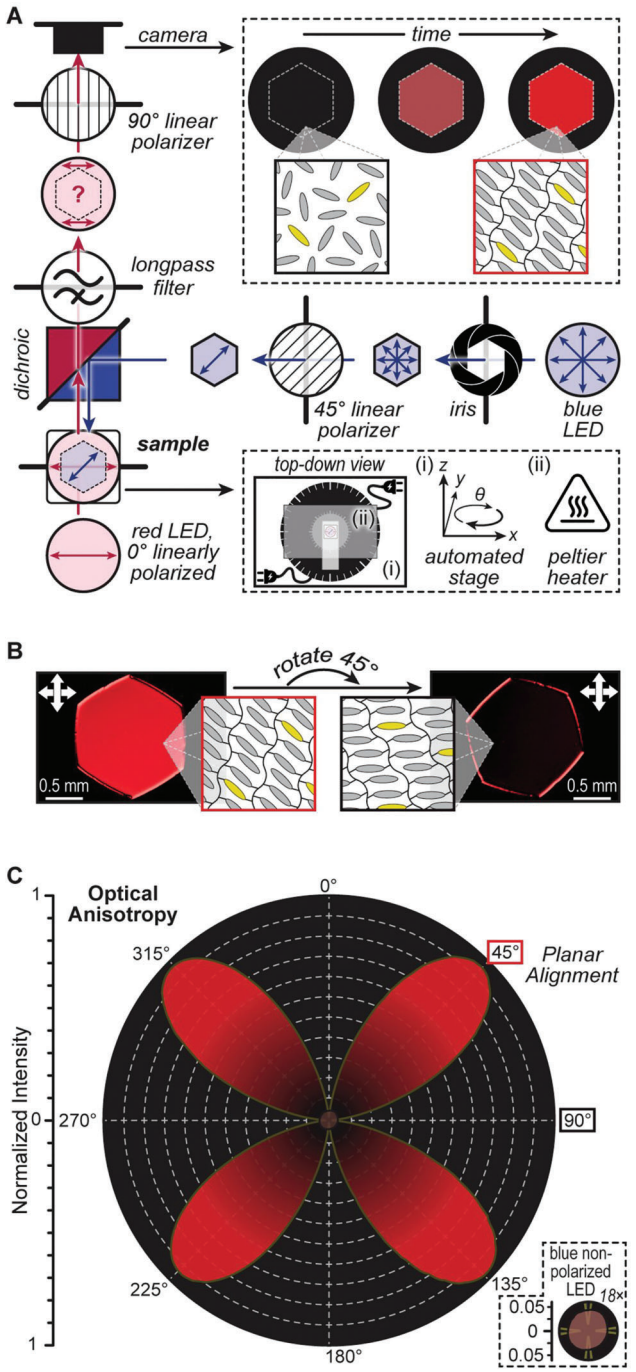

Figure 3. A) Schematic of polarized optical microscope setup used to induce, monitor, and characterize LC photoalignment. Red light along the vertical direction was selected to avoid azo-LC and BAPO absorption, while visualizing optical anisotropy during alignment. Inset in the upper right pictorially represents the photoalignment process and associated molecular-level orientation. B) Representative 6 µm thick sample prepared from RM-82:RM-23:azo-LC:BAPO (6.1:3.0:0.9:0.2), irradiated with a blue LPL for 10 min at an intensity of 30 mW cm^{-2}. C) Polar plot of hexagonal sample showing symmetric optical anisotropy that arises from in-plane LC alignment. Inset shows a polar plot for the same sample prepared with nonpolarized blue light, providing an isotropic LC polymer network. Camera exposure time for the inset was 18× longer relative to that used for the photoaligned sample.

region provided contrast and a frame of reference for quantifying optical anisotropy. Red light that passed through the sample was then sent through a 525 nm longpass filter that blocked blue light backscatter from reaching the camera. After the long pass filter, the transmitted red light passed through a linear polarizer set at 90° relative to the incident red LPL. For a more detailed description of this setup see the *Photo-Alignment and -Polymerization: POM Setup* section and Figure S15 in the Supporting Information.

As an initial experiment using this POM setup, a sample comprising RM-82:RM-23:azo-LC:BAPO at a 61:30:9:2 ratio was melted at 105 °C between glass slides that were separated by 6 µm spacers. Maintaining a temperature of 105 °C, the sample was then exposed to blue LPL for 10 min at an intensity of 30 mW cm^{-2} (Figure S17, Supporting Information). Viewing the product of this experiment on the POM revealed a bright red hexagon, which became dark upon rotating 45° (Figure 3B). Notably, the edges remained bright, which was hypothesized to arise from interfacial pinning effects by the surrounding isotropic medium and/or optical effects that occur upon polymerizing through the bulk of this relatively thick sample. This was further supported by more pronounced "edge-effects" for thicker (38 µm) samples (Figure S18, Supporting Information), which were the thickest samples that could be fully cured under the present conditions (Figures S19–S20, Supporting Information). Regardless of the thickness, the transition across the interface from bright to dark was sharp (Figure S18, Supporting Information), exemplifying good pattern fidelity.

Next, optical anisotropy was characterized by measuring brightness changes during a full 360° rotation of the sample (polar plot). The resulting polar plot was highly symmetric, which is indicative of uniform in-plane alignment (Figure 3C and Figure S21, Supporting Information). As a control, the same procedure was accomplished with nonpolarized blue light exposure (30 mW cm^{-2}). The resulting sample was completely dark between crossed polarizers, with no brightness change observed upon rotation (Figure 3C, inset). However, the outline of a hexagon was present using standard optical microscopy (i.e., not polarized), indicating that a polymer had formed resulting in a refractive index differential for contrast. This suggested that LPL was necessary for alignment in our process, while blue light – polarized or not – induced polymerization.

2.3. Optimizing Photo-Polymerization and -Alignment

To better understand the kinetics of the photoalignment process, the intensity of bottom-up red LPL was quantified over time during top-down blue LPL exposure on the POM (**Figure 4**A). These experiments revealed the presence of an induction period, or threshold time (t_{th}) of 0.46 ± 0.08 minutes (≈28 s) during which no increase in red light transmission was observed (Figure 4B, solid red line). Next, real-time Fourier-transform infrared (FTIR) spectroscopy was performed to characterize the acrylate conversion by monitoring the peak at 808 cm^{-1} (C=C stretch)[56] under identical conditions to that used for photoalignment (Figure 4B, dashed line). A similar induction period of 0.44 ± 0.06 minutes (≈26 s) was measured. Additionally, the rate of alignment (r_a = 1.0 ± 0.2 min^{-1}), characterized by the slope of intensity vs. time, was

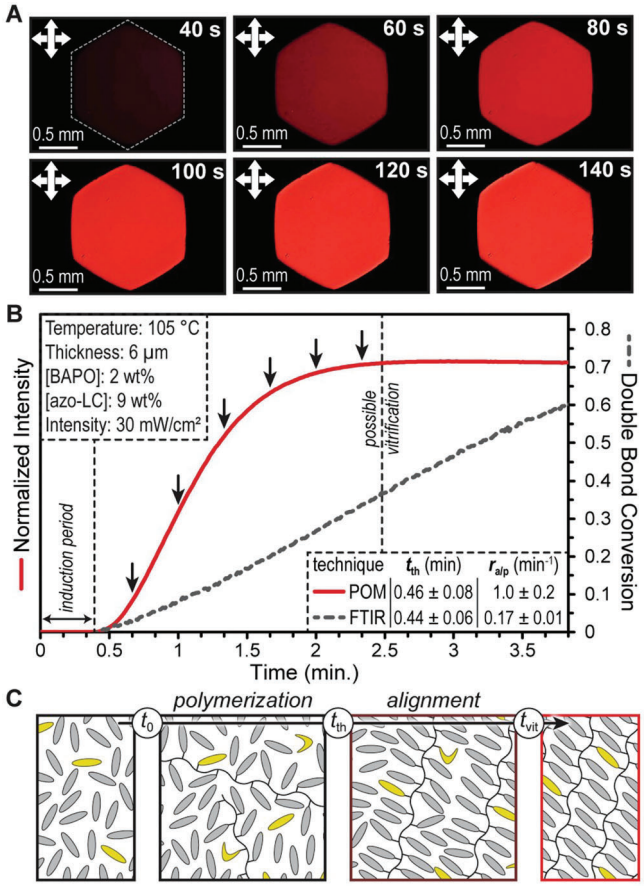

Figure 4. A) Representative example of in situ photoalignment monitoring using the custom POM setup, where an increase in red light intensity over time correlates to an increase in molecular anisotropy. B) Plot of normalized red-light intensity and double bond conversion as a function of time measured using POM and FTIR, respectively. Arrows correspond to images in part "A". Insets provide conditions (top left) and threshold time (t_{th}) and rates of alignment (r_a) and polymerization (r_p) (bottom right). Quantifiable metrics are provided as an inset in the bottom right, with values representing averages from three or more trials, including ± 1 standard deviation from the mean. C) Proposed four-stage mechanism where t_0 represents the time at which polymerization starts, t_{th} the time at which alignment starts, and t_{vit} the "vitrification" time or when alignment ceases.

greater than the rate of polymerization ($r_p = 0.17 \pm 0.01$ min^{-1}). This result provided further evidence that photo-polymerization and -alignment were coupled to one another.

The newly proposed mechanism followed four stages: 1) an induction period where the initial formation of radicals reacts with oxygen followed by 2) initiation and propagation (t_0). During the free radical chain-growth copolymerization, azo-LC units would be pinned alongside LCs (RM-82 and RM-23). This enabled 3) polarization-induced photoalignment (t_{th}) of azo-LC with possible amplification from neighboring (nonphotoresponsive) LCs. Finally, 4) "vitrification" (t_{vit}) was postulated to prevent further alignment through a restriction of mobility (Figure 4C). Note that "vitrification" is being used qualitatively to describe a decreased matrix mobility, but may not directly correspond with the formation of a "glass" by definition. Based upon this interplay between photo-polymerization and -alignment it was anticipated that both the kinetics and extent of optical anisotropy could be tailored by several parameters, including the concentration of photoinitiator ([BAPO]), intensity of incident irradiation (I_{LED}), and azobenzene concentration ([azo-LC]).

To examine the influence of these parameters on alignment, the kinetics (t_{th} and r_a) and maximum red LPL transmittance intensity (I_{max}) were characterized using the POM setup at a consistent sample thickness of 6 µm. Initially, the effect of [BAPO] was examined, holding constant [azo-LC] (9 wt%) and blue LED intensity (30 mW cm^{-2}) (**Figure 5**A). In general, it was found that decreasing the [BAPO] from 4 to 0.5 wt% resulted in an increase in t_{th} and I_{max}, but a decrease in r_a. These results can be rationalized by the proposed competition between photo-polymerization and -alignment, where lower [BAPO] results in a smaller r_p (observed by FTIR, Figure S22, Supporting Information). In turn, the smaller r_p increases the induction period and delays "vitrification", allowing for an increase in transmittance (I_{max}). Notably, [BAPO]'s < 0.5 wt% did not result in complete polymerization and alignment under these conditions (Figure S23, Supporting Information). Overall, a nearly 3× increase in I_{max} was demonstrated in going from a [BAPO] of 4 to 0.5 wt%.

Next, the effect of I_{LED} on optical anisotropy was characterized (Figure 5B). Increasing the intensity from 30 to 120 mW cm^{-2} resulted in a decrease in t_{th} and an increase in r_a with statistically insignificant changes in I_{max}. Moreover, this trend was consistent with 38 µm thick samples (Figure S24, Supporting Information). This behavior was rationalized by a simultaneous increase in both photo-polymerization and alignment kinetics. Finally, the effect of [azo-LC] was examined, finding that increasing the amount of azo-LC from 2 to 9 wt% resulted in an increase in t_{th} and I_{max}, without an observable trend on r_a. Notably, an [azo-LC] of 2 wt% resulted in a small increase in brightness, but no observable change in brightness upon rotating between crossed polarizers (Figure S25A, Supporting Information). This result indicates minimal alignment, but may also suggest that T_{NI} increases during polymerization with blue LPL. Therefore, samples may transition from a disordered isotropic state at the start of polymerization to an ordered nematic mesophase at the early stages of polymerization (t_{th}), facilitating photoalignment. This hypothesis is further supported by decreasing I_{max} at higher sample temperatures that are further from T_{NI} (Figure S10, Supporting Information). Increasing the [azo-LC] to 18 wt% precluded curing within 10 minutes of irradiation, likely due to the strong light absorption at these concentrations. From 4 to 9 wt% azo-LC the increase in t_{th} and I_{max} can be rationalized by an increase in relative photons absorbed for azo-LC:BAPO from ≈400–900×, respectively (Figures S13–S14, Supporting Information), decreasing the rate of radical formation and leading to a longer induction period and delayed "vitrification". Under optimized conditions of 2:1 RM-82:RM-23, 9 wt% azo-LC, 0.5 wt% BAPO, and 10 minutes of 90 mW cm^{-2} blue LED exposure (to ensure complete curing), the samples exposed with LPL showed a moderate dichroic ratio (R) of 1.27, which is equal to a dichroic order parameter (S) of 0.08, as measured using polarized UV-vis absorption spectroscopy (Figure S26, Supporting Information). In contrast, samples prepared using nonpolarized blue light exposure had an $R = 1.03$ and $S < 0.01$. This confirmed that the photoalignment process with LPL was effective at causing in-plane molecular reorientation, as previously suggested by the polar plot (Figure 3C).

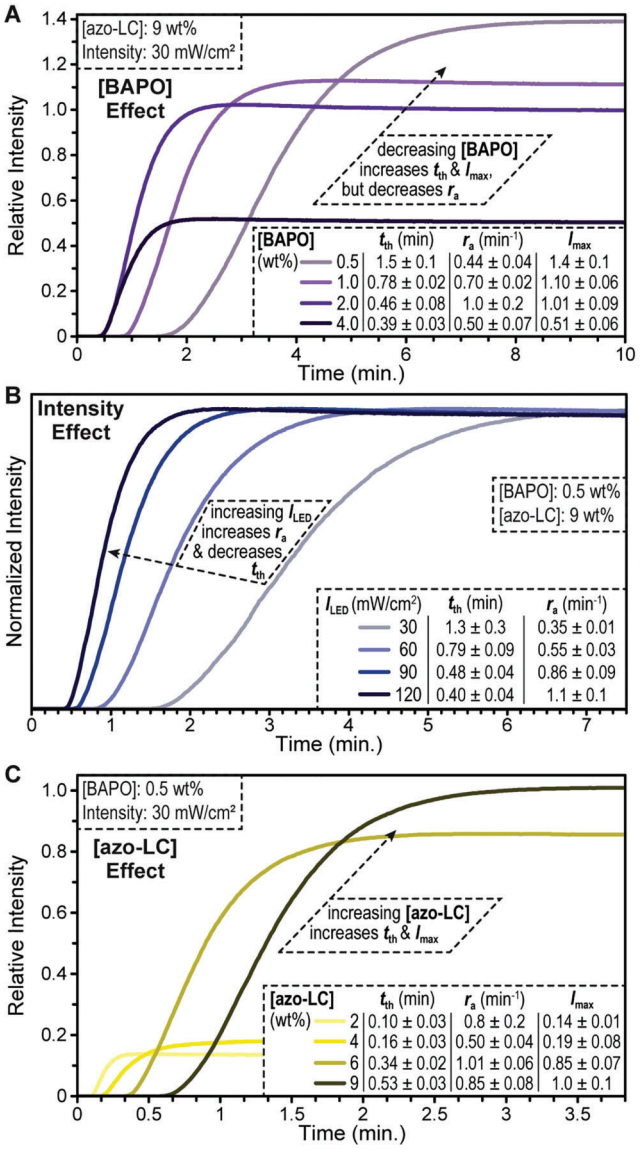

Figure 5. Effect of A) [BAPO], B) incident blue LPL intensity (I_{LED}), and C) [azo-LC] on threshold time (t_{th}), rate of alignment (r_a), and maximum transmitted red-light intensity (I_{max}) measured using the POM setup described in Figure 3A. All samples had a thickness of 6 µm with other constant parameters provided as an inset within a dashed box for each individual plot. Quantifiable metrics are provided as an inset in the bottom right, with values representing averages from three or more trials, including ± 1 standard deviation from the mean. The y-axis in part (B) has been normalized given that differences in I_{max} were insignificant.

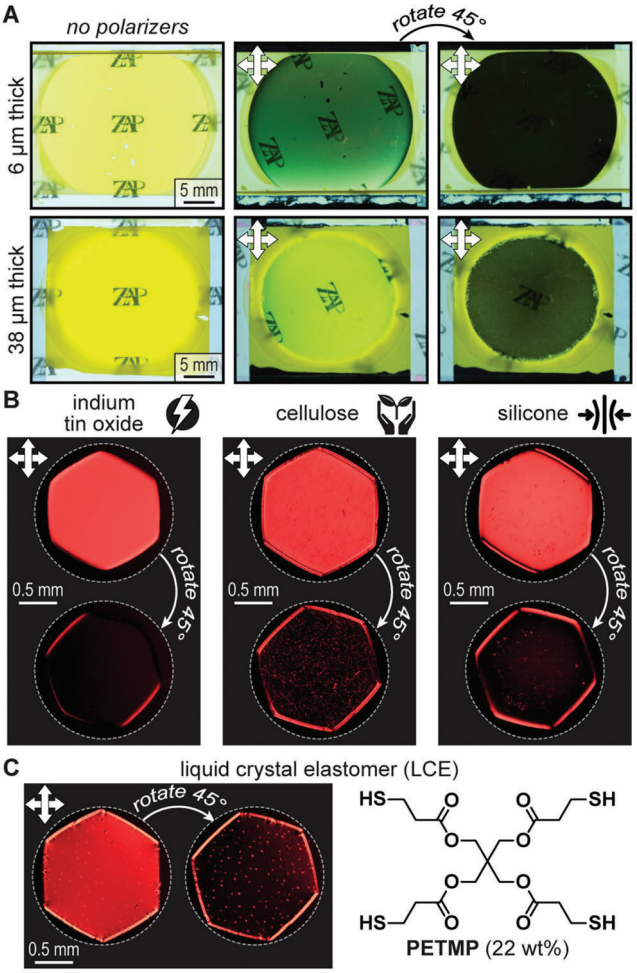

Figure 6. Scope of the present photoalignment process. A) Images of backlit 6 and 38 µm thick samples without and with crossed polarizers showcasing transparency and optical anisotropy, respectively. A constant camera exposure time was used for each image. B) POM images of photoaligned samples prepared on various substrates rotated between crossed polarizers, demonstrating substrate-independence. C) POM images of a photoaligned LCE, demonstrating matrix scope. PETMP = pentaerythritol tetrakis(3-mercaptopropionate).

2.4. Process Scope

The scope of the photoalignment process was further tested by examining the influence of sample thickness and substrate and LC matrix composition. Using the optimal conditions of 2:1 RM-82:RM-23, 9 wt% azo-LC, 0.5 wt% BAPO, and 10 minutes of 90 mW cm^{-2} blue LED exposure, optically anisotropic samples up to a thickness of 38 µm could be prepared (**Figure 6**A). Notably, the samples had high optical transparency, with transmittance exceeding 90% beyond 535 nm (Figure S27, Supporting Information). This was attributed to photoalignment occurring initially above T_{NI}, despite the nematic genesis that may be occurring upon polymerization.

Next, the bulk photoalignment process was applied to the same optimized LC composition (unless otherwise noted) on a variety of surfaces. Samples were prepared as 6 µm films between three functional substrates; conductive indium tin oxide (ITO) coated glass (with ITO facing the LC on both sides), biodegradable/compostable cellulose, and soft/elastomeric silicone (Figure 6B). For the latter two, a coverslip was used as the top surface for structural integrity (see *LC & LCE preparation* section in the Supporting Information for more details). Notably, 2 wt% BAPO was used for samples prepared on silicone and cellulose to overcome their higher oxygen permeability precluding free radical polymerization. After irradiation with blue LPL for

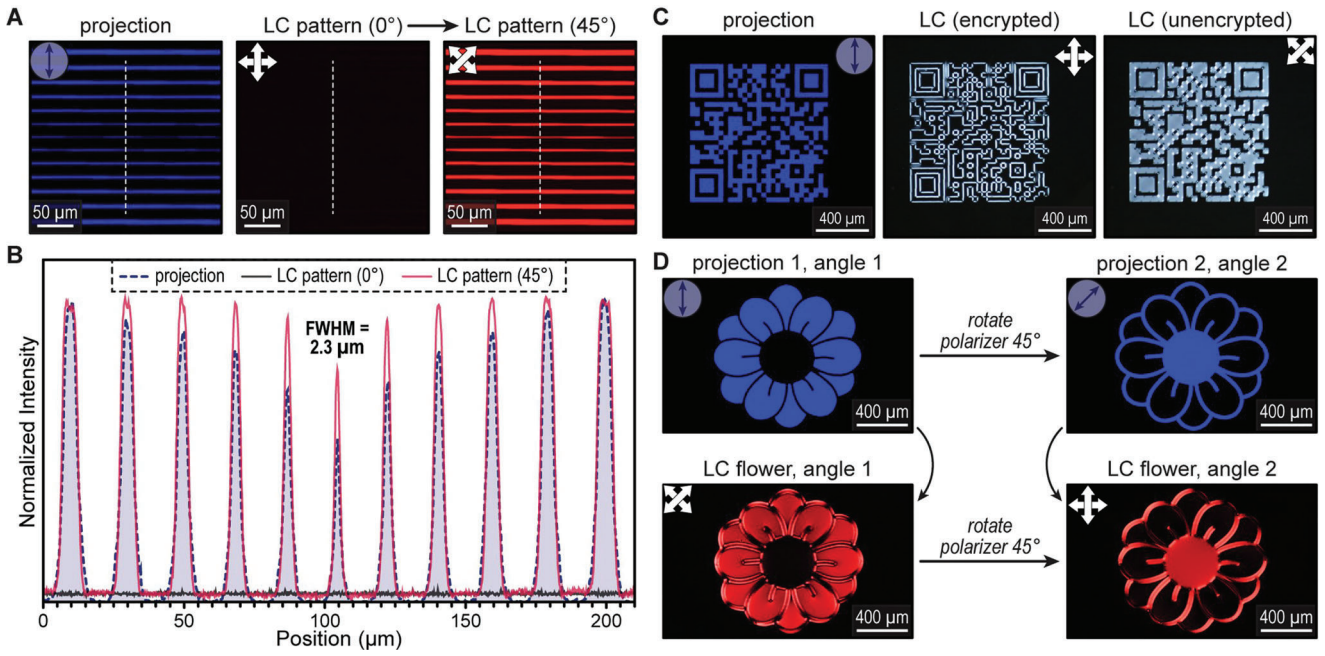

Figure 7. Photopatterning optical anisotropy using a POM equipped with a digital mirror device. A) POM images of equally spaced lines using a 10× objective. From left to right: projection (0° blue LPL reflected off of a mirror) and LC sample at 0° and 45° between crossed polarizers. B) Plot of line intensity across each image showing excellent pattern fidelity and a minimum feature size of 2.3 µm. FWHM = full width at half maximum. C) Encrypted QR code linking to the "ZAP Group Research" webpage. D) Multiangle photopatterning by sequential projections at disparate angles of blue LPL, showing a flower (projection 1) and it's inverse (projection 2) at 0° and 45°, respectively, along with the corresponding LC samples with multiangle alignment.

10 minutes, similar optical anisotropy – brightness changes upon rotating samples 45° between crossed polarizers – was observed relative to the all-glass substrates. These experiments exemplify the substrate independence of the present protocol.

To test the matrix scope, different sample compositions were examined. Specifically, alternative reactive mesogens or a tetrathiol chain transfer agent were incorporated into the bulk LC resin (Figure 6C). Replacing the diacrylate RM-82 (hexamethylene spacer) with RM-257 (trimethylene spacer) or replacing the monoacrylate RM-23 with RM-105 resulted in similar optical anisotropy to the original LC recipe (Figure 2A and Figure S28, Supporting Information). Moreover, incorporating 22 wt% pentaerythritol tetrakis(3-mercaptopropionate) into the following LC mixture resulted in the formation of a liquid crystal elastomer (LCE): 34 wt% RM-82, 34 wt% RM-257, 9 wt% azo-LC, and 0.5 wt% BAPO. Incorporation of the tetrathiol decreased the glass transition temperature from 75°C (original network) to 34 °C (LCE), as measured using differential scanning calorimetry and dynamic mechanical analysis (Figures S29–S30, Supporting Information). Additionally, the T_{NI} of the mixture was decreased from 97 °C to 55 °C as measured by POM (Figure S4B, Supporting Information). The LCE precursor mixture was heated to 70 °C, above the T_{NI}, and irradiating with 30 mW cm^{-2} for 10 min, resulting in a transparent, yet optically anisotropic film (Figure 6C, see *LC & LCE preparation* section in the SI for more details). Furthermore, the optical anisotropy was found to be stable upon heating to ≥200 °C (Figures S31–S32, Supporting Information). The present bulk photoalignment process is thus robust and nondiscriminatory, enabling a wide scope in thickness and both substrate and matrix composition.

2.5. Photo-Patterning

The implementation of light inherently facilitates spatial control, and we thus chose to examine the feature size and resolution limits of photopatterning using the current bulk alignment process (**Figure 7**). Equipping the custom POM with a top-down digital mirror device enabled projection through the objectives (see *LC Photo-Patterning* section in the SI for more details). Placing a polarizer in front of the sample allowed for photoalignment micropatterning. Using a 10× objective, equally spaced lines of decreasing full width at half maximum (FWHM) were projected onto the original 6 µm thick LC mixture (at 105 °C, with $I_{LED} = 90$ mW cm^{-2} for ≈3.3 minutes) to determine the minimum feature size (Figure 7A). Excellent transfer fidelity of optically anisotropic features was observed, and mapping the intensity across the images on the POM revealed a FWHM down to 2.3 µm, which represents 1-pixel width from the DMD (i.e., limit of projection) (Figure 7B). Furthermore, lines with decreasing spacing between them revealed a feature resolution of 3.6 µm, that is the smallest discernable edge-to-edge distance, which was also limited by the projection resolution (Figure S34 and Video S3, Supporting Information). Overall, this process uses readily available visible LEDs to rapidly pattern micrometer features across millimeter length scales, which can be further expanded using (automated) lateral stitching of images (Figure S38 and Video S4, Supporting Information), possible on most microscopes.

As a final proof-of-concept complex images were patterned to showcase the ability to program arbitrary shapes with potential applications for encryption and data storage. First, a micrometer-scale quick response (QR) code linking to our group's webpage

was patterned into the LC mixture (Figure 7C and Video S5, Supporting Information). Rotating the optically anisotropic QR code between crossed polarizers revealed that it was encrypted at all angles apart from those at intervals of 45° ± 10° relative to the original polarization angle of incident blue LPL (0°) (Figure S37, Supporting Information). Additionally, images containing multiple distinct angles of LPL transmittance were fabricated through a simple projection of sequential images and rotating the polarizer (or sample) between each projection. As an example, an LC flower image was created by first projecting one image followed by rotating the polarization angle of incident blue LPL by 45° and projecting the inverse image (Figure 7D). Notably, this bulk photoalignment process should be amenable to simultaneous multiangle patterning using a spatial light modulator, as previously demonstrated with surface-mediated photoalignment.[43] Upon rotating the LC sample between crossed polarizers, the two distinct images appear/disappear, highlighting the ability of the present process to create complex optically anisotropic patterns (Video S6, Supporting Information).

3. Concluding Remarks

In summary, a user-friendly LC photoalignment process was described, where in situ POM analysis enabled a systematic examination and optimization of the parameters that govern optical anisotropy. This study unveiled a unique cooperativity between photo-polymerization and -alignment that occurred upon irradiating a resin comprising an azobenzene LC diluted in a commercially available LC host matrix with relatively low intensity (≈30–90 mW cm^{-2}) blue LPL. The bulk photoalignment strategy provided rapid (<10 min), substrate-independent, and high-resolution (<5 μm features) patterning of optical anisotropy in thick (≈6–38 μm) and transparent LC networks. Building upon this foundation, the modular photoalignment and in situ, monitoring protocols can be applied to a wider range of LC chemistries, such as base-catalyzed thiol-Michael addition and cationic epoxy ring-opening polymerizations. Additionally, reducing the crosslinker content and further tailoring the absorption cross section between the azo-LC and photoinitiator has the potential to further increase the rate and extent of alignment (i.e., order parameter) as well as the maximum achievable thickness. This diversification will provide additional mechanistic insight into how composition influences photoalignment and order parameter. Furthermore, the ease of scalability will enable systematic studies that correlate localized molecular alignment to bulk mechanical properties. Overall, continued formulation optimization of this nascent protocol has the potential to enable the fabrication of next-generation soft actuators for biomedical applications and optical devices for data storage and encryption.

Supporting Information

Supporting Information is available from the Wiley Online Library or from the author.

Acknowledgements

The authors acknowledge primary support from the Air Force Office of Scientific Research under Grant No. FA9550-21-1-0115 (J.Z., J.S., Y.W., Z.A.P.). Partial support was provided by the Robert A. Welch Foundation under Grant No. F-2007 (Z.A.P.). AFRL authors acknowledge funding support from the Materials and Manufacturing Directorate under contracts FA8650-20-F-5409 and FA8650-22-F-5406 (C.P.A., Z.M.M., N.P.G.). The authors thank Dr. Mariacristina Rumi from AFRL for helpful discussions on this work.

Conflict of Interest

The authors declare no conflict of interest.

Author Contributions

J. Z. and J.S. contributed equally to this work. J.Z., J.S., and Z.A.P. performed the conceptualization; J.Z., J.S., Y.W., and Z.A.P. performed the methodology; J.Z., J.S., Y.W., C.P.A., Z.M.M., and K.N.L. performed investigation; J.Z. and Z.A.P. performed visualization; N.P.G. and Z.A.P. acquired funding; Z.A.P. acquired project administration; N.P.G. and Z.A.P. performed the supervision; J.Z. and Z.A.P. wrote the original draft; J.Z., J.S., Y.W., C.P.A., Z.M.M., N.P.G., and Z.A.P. reviewed and edited the final manuscript.

Data Availability Statement

The data that support the findings of this study are available in the supplementary material of this article.

Keywords

anisotropy, liquid crystals, photoalignment, photopolymerization, photopatterning

Received: July 28, 2023
Published online: August 22, 2023

[1] M. Yang, Y. Xu, X. Zhang, H. K. Bisoyi, P. Xue, Y. Yang, X. Yang, C. Valenzuela, Y. Chen, L. Wang, W. Feng, Q. Li, *Adv. Funct. Mater.* **2022**, *32*, 2201884.
[2] Y. Chen, C. Valenzuela, X. Zhang, X. Yang, L. Wang, W. Feng, *Nat. Commun.* **2023**, *14*, 3036.
[3] L. L. Ma, C. Y. Li, J. T. Pan, Y. E. Ji, C. Jiang, R. Zheng, Z. Y. Wang, Y. Wang, B. X. Li, Y. Q. Lu, *Light Sci Appl* **2022**, *11*, 270.
[4] J. Yang, X. Zhang, X. Zhang, L. Wang, W. Feng, Q. Li, *Adv. Mater.* **2021**, *33*, 2004754.
[5] X. Yang, C. Valenzuela, X. Zhang, Y. Chen, Y. Yang, L. Wang, W. Feng, *Matter* **2023**, *6*, 1278.
[6] H. Kawamoto, *Proc IEEE Inst. Electr. Electron. Eng.* **2002**, *90*, 460.
[7] E. K. Fleischmann, R. Zentel, *Angew. Chem., – Int. Ed.* **2013**, *52*, 8810.
[8] M. Schadt, *Annu. Rev. Mater. Sci.* **1997**, *27*, 305.
[9] H. W. Chen, J. H. Lee, B. Y. Lin, S. Chen, S. T. Wu, *Light Sci Appl* **2018**, *7*, 17168.
[10] V. P. Shibaev, A. Y. Bobrovsky, *Russ. Chem. Rev.* **2017**, *86*, 1024.
[11] J. Zhao, L. Zhang, J. Hu, *Adv. Intel. Syst.* **2022**, *4*, 2100065.
[12] K. M. Herbert, H. E. Fowler, J. M. McCracken, K. R. Schlafmann, J. A. Koch, T. J. White, *Nat. Rev. Mater.* **2022**, *7*, 23.
[13] V. G. Chigrinov, *Crystals* **2013**, *3*, 149.
[14] J. del Barrio, C. Sánchez-Somolinos, *Adv. Opt. Mater.* **2019**, *7*, 1900598
[15] V. Chigrinov, J. Sun, X. Wang, *Crystals* **2020**, *10*, 323.

[16] T. Seki, *Polym J* **2014**, *46*, 751.
[17] L. L. Ma, W. Hu, Z. G. Zheng, S. B. Wu, P. Chen, Q. Li, Y. Q. Lu, *Adv. Opt. Mater.* **2019**, *7*, 1900393.
[18] J. M. McCracken, B. R. Donovan, K. M. Lynch, T. J. White, *Adv. Funct. Mater.* **2021**, *31*, 2100564.
[19] T. H. Ware, M. E. McConney, J. J. Wie, V. P. Tondiglia, T. J. White, *Science* **2015**, *347*, 982.
[20] J. Uchida, B. Soberats, M. Gupta, T. Kato, *Adv. Mater.* **2022**, *34*, 2109063.
[21] J. P. F. Lagerwall, G. Scalia, *Curr. Appl. Phys.* **2012**, *12*, 1387.
[22] T. Ikeda, O. Tsutsumi, *Science* **1995**, *268*, 1873.
[23] W. Feng, D. Liu, D. J. Broer, *Small Struct.* **2021**, *2*, 2000107.
[24] M. Rim, D. G. Kang, D. Jung, S. I. Lim, K. M. Lee, N. P. Godman, M. E. McConney, L. De Sio, S. K. Ahn, K. U. Jeong, *Nanoscale* **2022**, *14*, 8271.
[25] P. Van Der Asdonk, P. H. J. Kouwer, *Chem. Soc. Rev.* **2017**, *46*, 5935.
[26] K. Ichimura, Y. Suzuki, T. Seki, A. Hosoki, K. Aoki, *Langmuir* **1988**, *4*, 1214.
[27] O. Yaroshchuk, Y. Reznikov, *J. Mater. Chem.* **2012**, *22*, 286.
[28] K. Ichimura, *Chem. Rev.* **2000**, *100*, 1847.
[29] K. Hisano, M. Aizawa, M. Ishizu, Y. Kurata, W. Nakano, N. Akamatsu, C. J. Barrett, A. Shishido, *Sci. Adv.* **2017**, *3*, e1701610.
[30] M. Ishizu, K. Hisano, M. Aizawa, C. J. Barrett, A. Shishido, *ACS Appl. Mater. Interfaces* **2022**, *15*, 14760.
[31] E. Ouskova, D. Fedorenko, Y. Reznikov, S. V. Shiyanovskii, L. Su, J. L. West, O. V. Kuksenok, O. Francescangeli, F. Simoni, *Phys. Rev. E* **2001**, *64*, 051709.
[32] H. Sakaino, D. J. Broer, S. C. J. Meskers, E. W. Meijer, G. Vantomme, *Angew. Chem., – Int. Ed.* **2022**, *61*, e202200839.
[33] M. O'Neill, S. M. Kelly, *J. Phys. D Appl. Phys.* **2000**, *33*, R67.
[34] V. Kumar, A. Nasrollahi, V. K. Baliyan, H. S. Park, M. H. Lee, S. W. Kang, *Opt. Mater. Express* **2018**, *8*, 2366.
[35] V. Kumar, A. Nasrollahi, H. S. Park, S. T. Shin, M. H. Lee, S. W. Kang, *J. Mol. Liq.* **2021**, *324*, 114778.
[36] K. Mukai, K. Imai, M. Hara, S. Nagano, T. Seki, *ChemPhotoChem* **2019**, *3*, 495.
[37] H. Zeng, O. M. Wani, P. Wasylczyk, R. Kaczmarek, A. Priimagi, *Adv. Mater.* **2017**, *29*, 1701814.
[38] J. Schneider, W. Zhang, A. K. Srivastava, V. G. Chigrinov, H. S. Kwok, A. L. Rogach, *Nano Lett.* **2017**, *17*, 3133.
[39] A. Nasrollahi, V. Kumar, M. H. Lee, S. W. Kang, H. S. Park, H. Lim, K. C Oh, J. J. Lyu, *ACS Appl. Mater. Interfaces* **2019**, *11*, 15141.
[40] V. Kumar, Z. Ye, H. Jiang, Y. Shi, K. Li, D. Gérard, D. Luo, Q. Mu, Y. J. Liu, *ACS Appl. Electron. Mater.* **2020**, *2*, 2017.
[41] M. E. McConney, A. Martinez, V. P. Tondiglia, K. M. Lee, D. Langley, I. I. Smalyukh, T. J. White, *Adv. Mater.* **2013**, *25*, 5880.
[42] T. Guin, M. J. Settle, B. A. Kowalski, A. D. Auguste, R. V. Beblo, G. W. Reich, T. J. White, *Nat. Commun.* **2018**, *9*, 2531.
[43] B. A. Kowalski, V. P. Tondiglia, T. Guin, T. J. White, *Soft Matter* **2017**, *13*, 4335.
[44] Z. G. Zheng, C. L. Yuan, W. Hu, H. K. Bisoyi, M. J. Tang, Z. Liu, P. Z. Sun, W. Q. Yang, X. Q. Wang, D. Shen, Y. Li, F. Ye, Y. Q. Lu, G. Li, Q. Li, *Adv. Mater.* **2017**, *29*, 1703165.
[45] H. Yu, T. Kobayashi, *Molecules* **2010**, *15*, 570.
[46] A. Shishido, *Polym J* **2010**, *42*, 525.
[47] T. Ube, H. Tsunoda, K. Kawasaki, T. Ikeda, *Adv. Opt. Mater.* **2021**, *9*, 2100053.
[48] C. Kawakami, M. Hara, S. Nagano, T. Seki, *Langmuir* **2023**, *39*, 619.
[49] Y. Chen, S. Huang, T. Wang, H. Yu, *Macromolecules* **2020**, *53*, 1486.
[50] A. Kudreyko, V. Chigrinov, G. Hegde, D. Chausov, *Crystals* **2023**, *13*, 965.
[51] S. Nagano, *Polym J* **2018**, *50*, 1107.
[52] G. T. Carroll, K. M. Lee, M. E. McConney, H. J. Hall, *J Mater. Chem. C Mater.* **2023**, *11*, 2177.
[53] H. Zhou, A. S. Kuenstler, W. Xu, M. Hu, R. C. Hayward, *Macromolecules* **2022**, *55*, 10330.
[54] A. S. Kuenstler, K. D. Clark, J. Read De Alaniz, R. C. Hayward, *ACS Macro Lett.* **2020**, *9*, 902.
[55] D. Broer, G. P. Crawford, S. Zumer, Eds., *Cross-Linked Liquid Crystalline Systems: From Rigid Polymer Networks to Elastomers*, CRC Press/Taylor & Francis Group, Boca Raton, FL **2011**.
[56] L. G. Lovell, K. A. Berchtold, J. E. Elliott, H. Lu, C. N. Bowman, *Polym. Adv. Technol.* **2001**, *12*, 335.